JOURNAL OF PROPULSION AND POWER
Vol. 16, No. 2, March–April 2000

Eulerian Approach for Unsteady Two-Phase Solid Rocket Flows with Aluminum Particles

Eric Daniel*
Université de Provence, 13453 Marseille CEDEX 13, France

To increase the specific impulse in a solid rocket motor, aluminum particles are embedded in the propellant formulation; combustion of these particles causes two-phase and reactive flow features. A model of unsteady compressible flow is presented, which includes particle-phase effects. The composition of gaseous combustion products of such a solid propellant involves many species and, to reduce the computational time, a reduced description is used for the gas phase. The particles are assumed to form a continuum; then, the dispersed phase is treated by an Eulerian approach. A basic description of aluminum combustion and the current general knowledge are presented. Aluminum combustion is computed by using Law's model, which assumes a steady vapor-phase diffusion flame; a D^n law giving the vaporized aluminum mass flow rate is also used. The computations are performed on a simple cylindrical port motor. After some computational verifications, a parametric study of several important quantities of the two-phase flow is carried out. The influence of particle injection velocity, initial diameter of aluminum particles, and effects of oxidizing species are analyzed.

Nomenclature

C_m = loading mass ratio
D = particle diameter, m
E = total energy, J
E_i = efficiency of oxidizer species
F_{g-p} = gas–particle drag force, N/m^3
L^* = characteristic motor length
L_{vap} = heat of phase change, J/kg
l_p = mean particle spacing, m
M = mass, kg
N = particle density number, m^{-3}
P = pressure, Pa
Q_{q-p} = gas–particle heat transfer, W/m^3
Q_1, Q_2 = reaction condensation heat, J
R = gas constant, J · K^{-1} · kg^{-1}
T_S = aluminum saturation temperature, K
$\boldsymbol{U}$ = velocity vector, m/s
u, v = components of velocity vector, m/s
Y = mass fraction
α = volume fraction
Γ = energy transfer, W/m^3
ρ = density, kg/m^3
ω = species production rate, kg · m^{-3} · s

Subscripts

g, p = gas, dispersed phase
prop = propellant
sat = saturation

Introduction

FOR many years the combustion process of metalized solid propellants has been studied by experimental, analytical, and numerical means. There is a renewed interest in the combustion of aluminum particles because this phenomenon is not yet well understood. Moreover, an understanding of this combustion process is necessary to predict the various phenomena occurring in a solid rocket motor (SRM), such as vortex shedding, propellant-burning rate response, alumina deposition, and erosion of thermal protection between the segmented propellants. Because of significant improvement in computational capabilities, the use of sophisticated combustion models for two- or three-dimensional internal flow modeling is feasible with appropriate assumptions. Others have considered the computation of steady-state reactive two-phase flows.[1,2] In those papers the dispersed phase was treated with a Lagrangian approach and the particle combustion model proposed by Hermsen,[3] incorporating a D^n law, was used for the temporal evolution of the particle diameter.

A different model is presented here, differing from both the numerical and the combustion models. Also, in follow-up studies, unsteady computations will be considered, and this is the reason why an Eulerian approach is used to describe the dispersed-phase behavior. It should be more efficient, in CPU time and memory requirements, than the Lagrangian method. Unsteady calculations are applied to study the motor instabilities as well as vortex-shedding phenomena. Such studies have been performed in the case of inert particles.[4] The propagation of an acoustic field in the two-phase flow inside a motor has been performed numerically and the results are compared with linear theory.

The model used here is a natural extension of the previous one for inert particles.[4] The crucial difference is the addition of the reactive features of the flow to the former model. This leads to a large number of gaseous species in the flow, as determined by an equilibrium chemical calculation of typical combustion of a propellant. It is not realistic to take into account all of the gaseous species and detailed behavior of particle-phase combustion processes. A reduced model for the propellant gas composition therefore is chosen to avoid computational time penalties. This requires preliminary calculations to obtain the chemical equilibrium composition in order to chose only three major species, each of which is a mixture of several elemental species. Moreover, the particle combustion process is quite complicated and not entirely understood. As discussed in the next section, only two kinds of models have been developed and generally are used for such applications. The first is Hermsen's model[3] and the second is the analytical Law model.[5] In the latter, a vapor-phase combustion is assumed,[5] to which some modifications have been made.[6]

In the following section the combustion models and the set of governing partial differential equations of the flow are presented. The numerical scheme is described briefly. For the numerical study the major parameters of the flow and the sensitivity of the results to them are identified. Numerical parameters (e.g., mesh refinement, time step) as well as physical parameters (e.g., heat of reaction, injection velocity of particles, initial diameter) also are considered.

Presented as Paper 98-3697 at the AIAA/ASME/SAE/ASEE 34th Joint Propulsion Conference, Cleveland, OH, 13–15 July 1998; received 13 November 1998; revision received 11 March 1999; accepted for publication 12 March 1999.

*Assistant Professor, IUSTI 5, rue Fermi. Member AIAA.

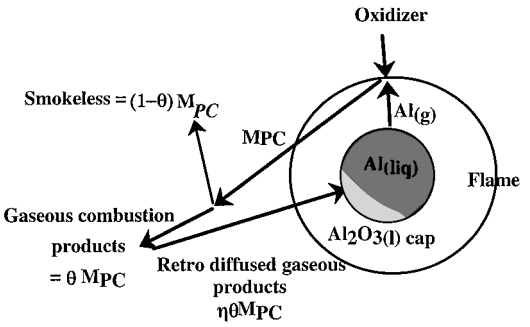

Fig. 1 Schematic of aluminum particle combustion process.

Combustion Model

The combustion of metal particles arising from those embedded in a solid propellant has been studied experimentally and theoretically. The first theoretical foundation was from Glassman[7] and was used as the starting point for analytical models. Because of their thermodynamic properties, which lead to a large specific impulse, the aluminum particles generally are preferred to other metal particles,[8] e.g., Be, Mg. The combustion process of such particles is assumed to be a vapor-phase diffusion control process. One of the major difficulties of modeling that combustion lies in the production of oxide smoke at the flame. The smoke is formed with submicron particles of liquid alumina. This is a very different process than the combustion of hydrocarbon droplets in air. In the model generally used, a fraction of the combustion products inwardly diffuses the aluminum particle to form an oxide (Al_2O_3) condensation surface, and another fraction forms some micron-sized smoke. However, some gaseous combustion products also exist in this process (Fig. 1). Note that initially the aluminum particles are covered by an oxide coating, which induces an ignition delay (this phenomenon is not included in the various models described below).

The phenomenology and modeling of the combustion are still being investigated, as presented in Refs. 9–11. Many of the complex phenomena that occur are not well understood (e.g., hollow spheres, spin, surface jets, and explosion). Also, the combustion seems to be very dependent on the experimental environment, ambient gas and oxidizer species, ignition method. In addition, the enveloping flame (with smoke) considerably hinders the investigation of the time-dependent particle behavior, requiring sophisticated diagnostic methods. The high-temperature flame ($\approx$3800 K) acts as a shield and prevents a good thermal analysis of the particle surface.

Two classes of models exist today. One is based on a correlation giving a D^n ($n = [1.5; 2]$) law for the time evolution of the particle diameter.[3] A second approach is based on the analytical Law's model.[5]

The first model—Hermsen's—only provides the mass flow rate of gaseous aluminum at the particle surface. A classical law is given by the following relation:

$$\frac{\mathrm{d}m_{\mathrm{Al}}}{\mathrm{d}t} = -\frac{\pi}{2}\rho_{\mathrm{Al}}\frac{k}{n}D^{3-n} \tag{1}$$

with $k = 8.3314 \times 10^{-5} P_m^{0.27}(100 \sum X_i)^{0.9}$, ($\mathrm{cm}^{1.8}/\mathrm{s}$). In this expression, P_m (psia) is the average pressure in the combustion chamber and X_i is the mole fraction of the oxidizer species. It must be emphasized that the oxidizer species are not specifically identified. Generally, CO_2, H_2O, and O_2 are considered. The 0.9 value of the exponent is imposed to fit the data with the observed combustion time. It is related to the notion of the efficiency of the aluminum combustion. One may first remark that this model does not provide any information about the condensed alumina at the surface particle, or the thermodynamic data. So, the fraction of condensed alumina must be imposed a priori. Note that this fraction can be divided into two parts: the first is supposed to form the characteristic spherical cap at the particle surface; the second part, formed by the alumina smoke, is included in the gas phase. This last point is justified because the thermal and dynamic states between the smoke and the gas are reached due to the small size of the smoke particles.

In the second model,[5] the mass and energy steady balance equations for a burning aluminum particle are solved by specifying the main quantities at the boundaries of the system, i.e., the particle surface and the flame. Most of the phenomena described earlier i.e., flame position, condensation surface, trapped condensed oxide at the flame, can be taken into account. This model has been improved over the years without really being questioned. The improvements concern the spherical cap on the particle and the variables' thermodynamic properties.[6,11] The solution of this analytical model leads to the value of the evaporated aluminum mass flow rate, namely, M_{Al} and the different mass fractions involved in the phenomenon. The total amount of combustion products, which are labeled as the $Al_2O_{3(g)}$ species, then is given by the relation $\dot{M}_{\mathrm{PC}} = (1 + \upsilon)\dot{M}_{\mathrm{Al}}$. In accordance with the phenomenology described by the scheme in Fig. 1, the vaporized part of the combustion products is equal to $\dot{M}_{\mathrm{PC,VAP}} = \theta\dot{M}_{\mathrm{PC}}$ from which the retrodiffused part is then $\dot{M}_{\mathrm{PC,VAP,RD}} = \eta\dot{M}_{\mathrm{PC,VAP}} = \theta\eta\dot{M}_{\mathrm{PC}}$. Obviously, the smoke part is $\dot{M}_{\mathrm{SM}} = (1 - \theta)\dot{M}_{\mathrm{PC}}$. The coefficient ν is the mass stochiometric coefficient of the elemental combustion reaction (2):

$$2\mathrm{Al}_{(g)} + \tfrac{3}{2}\mathrm{O}_{2(g)} \rightarrow \mathrm{Al}_2\mathrm{O}_{3(g)} \tag{2}$$

with $\nu = \frac{3}{4} \times (\frac{32}{27})$. Law's model allows the calculation of all fractions involved in the process. For more details about the solution, the reader is referred to Refs. 5, 6, 10, and 11. In the numerical model the boundary data are the gaseous temperature and the oxidizer mass fraction Y_{OX} at infinity, and the solution is $\dot{M}_{\mathrm{Al}}$, η, and θ. A coefficient is used to model the efficiency of the combustion.[11] The influence of this value is significant and is examined later.

Briefly, the drawbacks and advantages of each approach are summarized. The Hermsen model is based on a correlation from experimental data, giving the time evolution of the particle mass. The model can account for the combustion-chamber pressure and the efficiency of the oxidizer, but the model does not allow one to determine the alumina mass either on the particle or going into the gas phase as smoke. These two parameters must be imposed when numerical simulations are performed[1,2] what is done by successive attempts.

In contrast, Law's model can predict these different mass fractions and therefore this model can be considered to be a self-governing one. Note that it also leads to a D^n law of the diameter evolution in time, but when the combustion is completed, the diameter of the particle is not zero but equal to the alumina residual size. However, that model has the disadvantage of not taking into account the influence of the pressure except through physical-property variations, even though such an effect was pointed out earlier by Davis.[12] This model is also more CPU-time intensive but it is assumed to be more complete and easier to modify, and so, it is preferred in these simulations. However, the two models are compared in the simulation of a lab-scale motor flowfieldship).

Note that the Law model is still in use today to simulate the behavior of a single droplet. Widener and Beckstead[13] used the Brook's model, with modifications regarding the combustion mode, to compute the combustion in a propellant atmosphere. However, these models have the same roots. Another tendency appears in the use of the direct simulation of the combustion of a single aluminum particle.[14] The general flow equations (mass, momentum, and energy) plus a chemical mechanism are solved to obtain transient solution around one droplet in air. A new point in the model is a surface reaction involving $Al_{(g)}$, $AlO_{(g)}$ and $Al_2O_{(g)}$, but the question remains about how such accurate information (i.e., surface reaction) could be incorporated in general computational fluid dynamics codes.

Governing Equations

Let C_m be the aluminum-loading mass ratio in the propellant, $M_p = C_m M_{\mathrm{prop}}$, it can be shown that the particle volume fraction in the gaseous mixture is

$$\alpha_p = \frac{\rho_g}{\rho^*}\frac{C_m}{1 - C_m} = \kappa\frac{\rho_g}{\rho^*}$$

Generally, C_m does not exceed $\frac{1}{3}$, which leads to $\alpha_p \approx 10^{-4}$. If the mean particle spacing in a homogeneous mixture is assumed to be given by $D/\alpha_p^{1/3}$, then $l_p/L^* \ll 1$; thus the two-phase flow is a dilute one in the configurations studied.[15] In the governing equations of the dispersed phase, the pressure term can be neglected: Information travels in the flow only via particle trajectories. About the gaseous volume fraction, the following assumption also can be used: $\alpha_{(g)} = 1 - \alpha_p \approx 1$. Then the coupling between the gas phase and the dispersed phase is only due to interphase transfer terms such as drag, mass, and heat transfer.

In the gas phase, dissipative effects are neglected compared to the previous two-phase terms. However, the viscosity terms should not be negligible near the walls. In the combustion chamber, this zone corresponds to the neighborhood of the surface propellant, where the two-phase exchange terms are dominant because of large nonequilibrium conditions. In the diverging part of the nozzle, the Euler description of the gas flow cannot track the viscous boundary layer, but this topic is excluded from the current investigations.

Then, for this phase the governing equations are

$$\frac{\partial \rho_g \boldsymbol{U}_g}{\partial t} + \nabla \cdot (\rho_g \boldsymbol{U}_g \boldsymbol{U}_g + PI) = \boldsymbol{F}_{g-p} + \Gamma_m \boldsymbol{U}_p \tag{3}$$

$$\frac{\partial \rho_g \varepsilon_g}{\partial t} + \nabla \cdot (\boldsymbol{U}_g[\rho_g \varepsilon_g + P]) = \boldsymbol{F}_{g-p} \cdot \boldsymbol{U}_p + \Gamma_{\text{ener}} + Q_{q-p} \tag{4}$$

$$\frac{\partial \rho_{g,i}}{\partial t} + \nabla \cdot \rho_{g,i} \boldsymbol{U}_g = \dot{\omega}_i \tag{5}$$

with $\sum \rho_{g,i} = \rho_g$ and $P = \rho_g R T_g$

Based on the assumptions made, the dispersed-phase equations are[15,16]

$$\frac{\partial \rho_p \boldsymbol{U}_p}{\partial t} + \nabla \cdot \rho_p \boldsymbol{U}_p \boldsymbol{U}_p = -\boldsymbol{F}_{g-p} - \Gamma_m \boldsymbol{U}_p \tag{6}$$

$$\frac{\partial N}{\partial t} + \nabla \cdot N \boldsymbol{U}_p = 0 \tag{7}$$

$$\frac{\partial \rho_p \varepsilon_p}{\partial t} + \nabla \cdot \rho_p \boldsymbol{U}_p \varepsilon_p = -Q_{g-p} - \Gamma_{p,\text{ener}} \tag{8}$$

$$\frac{\partial \rho_{p,i}}{\partial t} + \nabla \cdot \rho_{p,i} \boldsymbol{U}_p = \dot{\omega}_{p,i} \tag{9}$$

with $\rho_{p,i} = \rho_{\text{Al}}$ or $\rho_{\text{Al}_2\text{O}_3}$.

Species Definition

The two last particular species equations express the simultaneous presence of alumina and aluminum in the particle phase, whereas Eq. (7) concerns the global conservation of the number density because the breakup or coalescence phenomena are omitted. It is assumed that the particles formed at the flame around the aluminum particle are included in the gaseous phase due their small size. The diameter is also small enough to allow for thermal and dynamic equilibrium.

It is important to identify the different species making up the propellant combustion gas. The total amount of species could be quite large and it is not realistic in an unsteady code to follow the behavior of each individual gaseous species and the dispersed phase, and take into account the reactive aspects as well. Moreover, many of the chemical reactions are unknown, and the corresponding production terms cannot be expressed. The propellant gas phase then is assumed to be made up only of three major species: Inert I, oxidizer OX, and the combustion products PC. Typically, the oxidizer components are a mixture of CO_2, H_2O, and O_2 mixture. To obtain the inert mixture, one compares the composition of a gas propellant with and without aluminum. The third species is formed by all of the others, given by an equilibrium calculation. The Al_2O_3 smoke is included in the last one. The thermodynamic properties now can be obtained from the JANNAF tables (and here they are assumed to be constant). The smoke is inserted in the PC species through a modification of the C_p and the molar weight. That is, let

$$K = \frac{\rho_{\text{smoke}}}{\rho_{\text{PC},G}},$$

Then,

$$R_{\text{PC}} = \frac{R_{\text{PC},g}}{1+K}, \qquad C_{p\text{PC}} = \frac{(C_p)_{\text{PC},g} + K C_{p,\text{smoke}}}{1+K} \tag{10}$$

Mass Production Terms

The mass production rates $\dot{\omega}_{p,i}$ are obtained from Eq. (1) if the Hermsen model is used or from Law's model. With the latter, the input data are only the mass fraction of the oxidizer species and the ambiant gas temperature. This model was modified to take into account the oxide cap on the particle, which decreases the combustion rate. The production/destruction terms for the gaseous species are obtained directly by assuming a stochiometric reaction between aluminum and oxidizer species[10,11,17] (no chemical kinetic mechanism is involved here). Then, the terms $\dot{\omega}_{\text{PC}}$ and $\dot{\omega}_{\text{OX}}$ are computed directly from $\dot{\omega}_{p,\text{Al}}$, ν, θ and η values .

Because the OX is a mixture of elemental components, it is convenient to introduce an oxidation efficiency in the form $Y_{\text{OX},\infty} = E \cdot Y_{\text{OX}}$. For example, the simplest way is to count the number of O_2 moles that each of the components (CO_2, H_2O, O_2 . . .) can produce. As indicated by Brooks and Beckstead,[11] this calculation can be improved by taking into account the diffusivity and the heat of formation. The constants E_i are adjusted to obtain a good combustion time for an O_2–H_2O–CO_2 mixture. In Marion's work,[10] a similar calculation is provided, including a temperature and pressure dependence for these coefficients. Some typical values are given in Table 1. Thus, the effective oxidizer mass fraction needed in the combustion model is calculated by the relation

$$Y_{\text{OX},\infty} = \sum E_i Y_i \tag{11}$$

Source Terms of the Energy Equation

A difficulty in the modeling occurs when defining the energy of the mixture. For heterogeneous combustion, involving gas and particles, there are two successive phase changes: the aluminum vaporization and the alumina condensation. As shown next, the magnitude of the condensation energy is the same order as the heat of combustion. If the total energy is constant because the gas–particle system is isolated, two distinct conservation energy equations are needed because the temperature of the gaseous phase is different than that of the dispersed phase. So, in contrast to a gaseous combustion, the heat released by the chemical reactions appears as a source term on the right-hand side of the equations.

For the dispersed phase the reference energy is chosen on the liquidus of the aluminum and of the alumina, which means that the aluminum particles entering the flow are at the saturation temperature:

$$\varepsilon_p = Y_{p,\text{Al}} \varepsilon_{p,\text{Al}} + Y_{p,\text{Al}_2\text{O}_3} \varepsilon_{p,\text{Al}_2\text{O}_3} \tag{12}$$

with $Y_{p,i} = \rho_{p,i}/(\rho_{p,\text{Al}} + \rho_{p,\text{Al}_2\text{O}_3})$, the mass fraction of ith species of the dispersed phase. It is assumed that the energy required to maintain the aluminum at the liquid state and to vaporize it is provided by the radiative transfer with the flame envelope. The energy equation of the dispersed phase does not pose any problem when all of the thermodynamic quantities are constant, such as T_{sat}. However,

Table 1 Efficiency of oxidizing species

	Efficiency			
Reference	O_2	H_2O	CO_2	$T\infty$, K
10	1	0.67	0.174	4000
11	1	0.533	0.135	2500

when pressure variation is taken into account, the thermodynamic variables are not well known (i.e., T_{sat}, L_{vap}) and it is nearly impossible to obtain the correct temperature saturation by solving the energy equation. In this case, the energy equation is reduced to $T_{sat}(P)$, but Eq. (8) must be used when the combustion process stops.

Gas-Phase Energy-Balance Equation

The fuel is not a component of the gas phase (aluminum vapor), and then it is not possible to include this component in the energy equation. The heat released by the aluminum combustion must appear as a source term. Ignoring the kinetic energy and the heat transfer with particle surface, and if the gas is a closed system, we should have

$$D_t\rho_g e_g = 0 \qquad \text{with} \qquad e_g = \sum Y_i e_i^0 + \int Cv_i \, dT$$

or

$$D_t\rho_g e_g = D_t\rho_g \sum Y_i \int Cv_i \, dT + D_t\rho_g \sum Y_i e_i^0 = 0 \tag{13}$$

let

$$D_t\rho_g \sum Y_i \int Cv_i \, dT = -D_t\rho_g \sum Y_i e_i^0 \tag{14}$$

Because the gaseous aluminum does not appear in the sum term on the right-hand side of Eq. (14), the heat of reaction cannot be defined. Besides, the real chemical reaction is not specified and a part of the combustion products are in a condensed form (smoke), and so, it is rather difficult to make this term appear in the equation. The energy equation then is written as

$$D_t\rho_g \varepsilon_g = D_t\rho_g \sum Y_i \int Cv_i \, dT = \Gamma_{g,\text{ener}} \tag{15}$$

$\Gamma_{g,\text{ener}}$ is determined hereafter.

The aluminum combustion reaction can be assumed to have the following chemical mechanism:

$$2Al + 3O_2 \rightarrow Al_2O_{3(g)} + Q_1 \tag{16}$$

$$Al_2O_{3(g)} \rightarrow Al_2O_{3(liq)} + Q_2 \tag{17}$$

Many equivalent formulations can be found for the energy source term. The choice is reported on the available data. In this paper, this term is calculated by examining the total amount of energy per unit time, added to or substracted from the gas phase, by the mass transfer of each pseudospecies. For example, the term $\dot{M}_{OX}e_{OX}(TS)$ is lost by the gas phase but $\dot{M}_{SM}e_{SM}(TS)$ and $\dot{M}_{PC,VAP}e_{PC,VAP}(TS)$ are accounted as a gain. If we use the relation between the different mass flow rates and the definitions

$$Q_1 = \dot{M}_{Al}q_1 = \dot{M}_{Al}e_{Al}(TS) + \dot{M}_{OX}e_{OX}(TS) + \dot{M}_{PC}e_{PC}(TS) \tag{18}$$

the heat released by the combustion reaction per unit time, the classical definition of the heat of phase change $L_{vap} = e_{i,g}(TS) - e_{i,liq}(TS)$, then we find the total amount of the energy supplied in the gas phase:

$$\Gamma_{g,\text{ener}} = -\dot{M}_{OX}e_{OX}(TS) + \dot{M}_{SM}e_{SM}(TS) + \dot{M}_{PC,VAP}e_{PC,VAP}(TS) \tag{19}$$

or

$$\Gamma_{g,\text{ener}} = \dot{M}_{Al}([L_{vap}(Al) + q_1](1-\eta)\theta - ve_{OX}(TS) + (1-\theta)q_2) \tag{20}$$

The different heats of reactions (16) and (17) are computed from chemical equilibrium calculations in which several species are included (Al, AlO, Al_2O, AlO_2 ...) (Refs. 10 and 18). To obtain q_1 one has to consider a pseudoequilibrium, because $Al_2O_{3(g)}$ is a fictitious species. Law wrote this equilibrium as follows:

$$Al_2O_{3(g)} \leftrightarrow 2AlO + 0.5O_2 \tag{21}$$

Computing the heat of reaction at the aluminum saturation temperature leads to a value of q_1 equal to 2.104 kcal/g Al. The calculation of a Al_2O_3 dissociation proposed by Glassman,[19] which includes more realistic species, such as AlO, Al_2O, Al_2O_2, leads to $q_1 = 0.68$ kcal/g Al. The difference observed can be explained by the different species appearing in the equilibrium reactions, but the difference is noticeable. Typical values for q_2 are 7.31 kcal/g Al or 8.22 kcal/g Al (Refs. 5, 19, and 17).

Expressions for Mass, Heat, and Drag Force

In addition to the energy transfer due to the mass transfer, convective heat exchange and a drag force exist between the gas phase and the dispersed phase. To take into account the influence of relative velocity on the mass transfer, this term is multiplied by the Sherwood number (Sh) as indicated by the following correlation:

$$\omega_{p,i} = \varpi_{p,Al}\, Sh \qquad \text{with} \qquad Sh = 2 + \frac{0.555 Re^{\frac{1}{2}} Sc^{\frac{1}{3}}}{\left[1 + 1.232/\left(ReSc^{\frac{4}{3}}\right)\right]^{\frac{1}{2}}} \tag{22}$$

The latter is a correlation provided by Faeth[20] that is valid for a large range of Reynolds numbers. This Sherwood number is based on the local relative velocity and the particle diameter. The Lewis number is assumed equal to unity, so that the Schmidt number is equal to the Prandtl number. Then, the same correlation as Eq. (22) is used to compute the Nusselt number, and so, the convective heat transfer around an isolated particle is

$$Q_{g-p} = N\pi DNu\lambda_g(T_p - T_g)$$

The drag force is given by a classical relation[21]:

$$\boldsymbol{F}_{g-p} = (C_d/8)\pi D^2\rho_g \|\boldsymbol{U}_p - \boldsymbol{U}_g\|(\boldsymbol{U}_p - \boldsymbol{U}_g)$$

with

$$\begin{aligned} C_d &= (24/Re)(1 + Re^{0.66}/6) \qquad \text{if} \qquad Re < 10^3 \\ C_d &= 0.424 \qquad \text{if} \qquad Re \geq 10^3 \end{aligned} \tag{23}$$

Numerical Procedure

Methods that are second-order accurate in space and time are required to solve the set of partial differential equations. The method must be explicit to obtain physical transient solutions. A restriction on the time step exists, which is given by the classical Courant–Friedrichs–Lewy criterion. This time step has proven to be small enough compared to the dispersed-phase characteristic time.

A numerical method used for the study of inert two-phase flows[4] has been developed to take into account the reactive features. This method was based on the well-known MacCormack scheme, which is very efficient for such flows.[22] It has the drawback of requiring some artificial viscosity to avoid spurious oscillations due to its second-order nature. These terms are quite complex—second- and fourth-order—and involve numerous coefficients determined by numerical experiences.[23,24] A finite volume method, based on a total variation diminishing (TVD) scheme is then developed, because it seems more general. The scheme is based on the MUSCL–Hancok methodology,[25] which is presented later briefly. The system of equations is written under a conservative form:

$$\frac{\partial U}{\partial t} + \nabla \cdot F(U) = H \tag{24}$$

The finite volume method is applied to the homogeneous part of the system; that is,

$$\frac{\partial U}{\partial t} + \nabla \cdot F(U) = 0$$

The numerical approach requires three successive steps. First, the conservative variables are extrapolated from the center to the boundary of the cell. A piecewise linear variation is assumed; then, the

slope of the conservative variables is calculated. On a given interface k, two values of the conservative variables are obtained: $U_i^{k,L}$ and $U_i^{k,R}$ the values at the left and at the right, respectively, of the cell boundary.

The second step consists in computing the evolution over an half time step of the variables inside a control volume:

$$\tilde{U}_i = U_i - \frac{\Delta t/2}{\Omega_i} \sum_{k=1,N_{\text{face}}} \left[F(U)_i^{k,L}\right] \boldsymbol{l}_k \cdot \boldsymbol{n}_k \tag{25}$$

With these new data, the fluxes are obtained by the means of an exact Riemann solver for both phases. The solution is $\tilde{U}^k = f(\tilde{U}^{k,L}, U^{k,R})$ and then the finite volume formula is applied:

$$\bar{U}_i^{n+1} = U_i^n - \frac{\Delta t}{\Omega_i} \sum_{k=1,N_{\text{face}}} F(\tilde{U}^k) \boldsymbol{l}_k \cdot \boldsymbol{n}_k \tag{26}$$

During the first step, a limitation of the slopes is performed to ensure a TVD property of the method. Classical slope limiters are included in the method and Van Leer's is the one used in this paper. Note that the algorithm is used for both phases; only the Riemann solver differs according to the phase considered.

An additional step is necessary to obtain the solution at the next-level time, U^{n+1}, which consists of integrating the source terms by the means of an ordinary differential equation solver:

$$U^{n+1} = L_s(\bar{U}^{n+1})$$

with

$$L_s(U) \equiv \frac{\mathrm{d}U}{\mathrm{d}t} = H$$

The L_s operator may be the second- or fourth-order Runge–Kutta method.

Boundary Conditions

The numerical boundary-condition treatment is achieved with classical methods. Three boundary conditions may be encountered in such problems: wall, outflow, and injection (Fig. 2). Because of its inviscid nature, a slip condition is used for the gas phase as well as for the dispersed phase.[23,26] The outflow being a supersonic one, a first-order extrapolation can be utilized. This procedure is used again for the dispersed phase. On the propellant surface, all of the particle quantities are imposed: diameter, temperature, and mass flow rate. An ambiguity remains for the particle injection velocity, which will be the topic of a parametric study. Here, the gas mass flow rate and temperature are fixed. An isentropic relation is used to link these two injection parameters with the internal flow (due to the subsonic regime).

Predicted Results

The aim of this work was to examine the performance of the numerical model as well as to study the effect of several basic parameters of the current flow. So, simulations of a lab-scale-motor flowfield, defined in Ref. 27, were performed. This small motor consists of a simple combustion chamber and a converging diverging nozzle (Fig. 2). It was already used for the simulations of one-phase[27] and two-phase inert flows[24] to study flow stability. The computational domain associated with this small motor allows quick computations. Three meshes are defined; a coarse one (98 × 15), an intermediate one (98 × 30) and a refined one (131 × 27). The CPU time required is then quite reasonable for a parametric study. Even though the motor is a cylindrical one, the calculations are for a planar geometry. Axisymmetric calculations would lead to little additional information about the basic parameters of the two-phase reactive flow and would increase the computational time.

A brief comparison between the Law and the Hermsen models is first presented to show that they provide similar results. Then, Law model is used even though many quantities related to aluminum combustion are not well known. As mentioned previously, the heat of reaction q_1 may differ according to the calculation method, and the aluminum heat of vaporization is known for only several pressure. Thus, a parametrical study cannot be exhaustive. Necessary data for the computation were fixed to typical values commonly used. Some of them are reported in Table 2. These values were proposed by Law or reported in Refs. 5, 6, and 17. The oxidizer species is a CO_2–H_2O mixture with the mass fractions, respectively, $Y_{CO_2} = 0.3666$ and $Y_{H_2O} = 0.644$ (oxygen appears in negligible quantity). The combustion efficiency E is calculated by the relation $E = E_{CO_2} Y_{CO_2} + E_{H_2O} Y_{H_2O}$, with data extracted from Table 1. In the case of no particular specification, E is assumed to be a constant equal to unity.

The parametric study can be performed after a mesh refinement analysis is carried out for a particular case. The effects of the injection velocity, which remains an unknown, the influence of the initial particle diameter, and the combustion efficiency parameter E are examined. As mentioned, all of the thermodynamic quantities were unvaried. The major influences were studied on simple but quite relevant cases.[11,17] It is clear that the data imposed are still questionable, but the aim of the paper is not a stricto sensu prediction of an SRM flowfield, but, instead, is to establish solutions to a numerical model with reasonable assumptions.

General Case

In the case of the two-phase calculation, a total mass flow rate is imposed as well as the loading mass ratio of aluminum. The total mass flow rate is $\dot{M}_t = (1 - C_m)\dot{M}_g + C_m \dot{M}_p$. The value of $\dot{M}_t$ is equal to 16 kg · m^{-2} · s^{-1} and $C_m = 18\%$, a typical value in SRMs.[23]

As shown in Fig. 2, the gaseous and dispersed phases are injected through a surface that bounds the combustion chamber. The first calculation is for 30-μm aluminum particles, which burn in the flow. The combustion process is modeled with both the Law and Hermsen models. In the latter, the η and θ fractions defined earlier must be imposed. Sabnis and colleagues[1] analyzed the data of Salita's experiments and concluded that 20% of the alumina produced is found on the particle spherical cap. The remaining 80% is assumed to be included in the gas as smoke. A calculation using these proportions leads to a maximum temperature of about 6300 K, which is not realistic. Some gaseous combustion products actually are admitted in the combustion description and this decreases the amount of smoke. A fraction of the gaseous combustion products equal to 20% leads to results in accordance with thermochemical calculations. The difference observed is due to the high value of the alumina heat of condensation q_2. That shows that use of the Hermsen model requires several iterations.

Table 2 Typical thermochemical data

Q_1	Q_2	L_{vap}	Unit
2.10	7.31	2.58	kcal/g Al

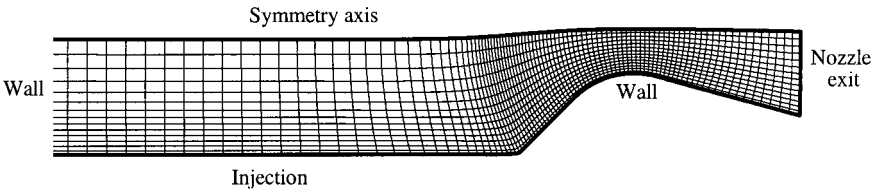

Fig. 2 Mesh for scale lab motor with the different boundary conditions (total length = 1 m, combustion chamber length = 0.66 m, maximum radius = 0.16 m, 98 × 15 coarse mesh is displayed).

In Fig. 3, the evolution of the ratio $\dot{M}_{t,\text{exit}}/\dot{M}_{t,\text{injected}}$ is plotted ralative to time. It was established that when the steady state is reached, the global mass balance is satisfied, whichever model is used. This test is an important one because the equations and the combustion phenomena are quite nonlinear. It is also a good way to check the validity of the numerical algorithm.

In Fig. 4, the particle diameter contours obtained with the Hermsen model are displayed. The end of combustion is observed at about half of the motor radius. Note that the residual alumina size is not negligible: The aluminum particles turn into alumina particles that become inert. At the nozzle exit the average diameter is equal to 19.3 μm. In the diverging part of the nozzle, a classical particle-free zone is observed.

In the following, the Law model is used in every computation. The influence of a grid refinement is first analyzed on the results. Three different meshes were utilized: a coarse one (98 × 15), an intermediate one (98 × 30) and a fine one (131 × 50). The different grids represent the same motor: The total length is 1 m, the combustion chamber length is 0.66 m, and its radius is 0.16 m. Whatever the grid, the mass conservation was attained at steady state. This criterion is not sensitive enough to establish the possible influence of the grid refinement. Some other, more characteristic, variables are the studied:

1) The combustion thickness δ is defined as

$$\delta = \frac{H_{\text{comb}}}{R_{\max}}$$

H_{comb} is the distance from the propellant surface where the combustion occurs and $R_{\max}$ is the combustion chamber radius. When the particles burn, in the present model, the dispersed-phase temperature is the aluminum saturation temperature and combustion is assumed to be over when a particle temperature change is detected.

2) The combustion time τ_c is computed from the steady-state results: An average Lagrangian trajectory of a pseudoparticle is computed from the propellant through the exit nozzle. This post-treatment also allows computation of the average diameter evolution over time.

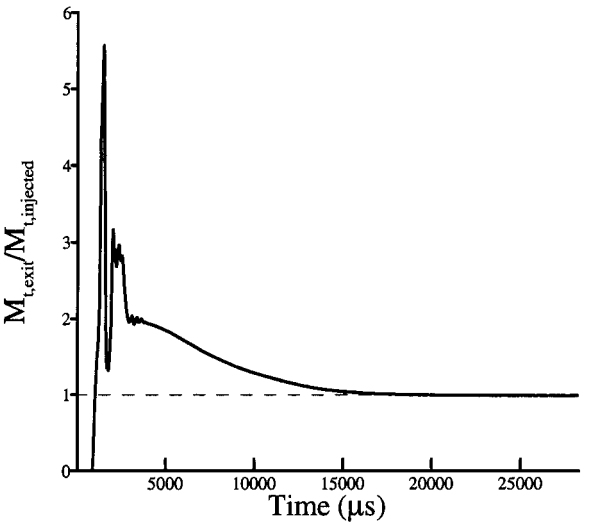

Fig. 3 $\dot{M}_{t,\text{exit}}/\dot{M}_{t,\text{injected}}$ vs time (——, unsteady evolution from two-dimensional computation; – – –, theoretical steady-state value).

3) The average temperature and pressure in the combustion chamber also were calculated. The averaging procedure is quite simple and is achieved on the discrete values from the surface propellant to the axis indices ($j = 1 \cdots N_Y$) and along the surface propellant ($i = 1 \cdots N_{\text{injection}}$).

For these comparisons the typical thermodynamic values were used. The dispersed injection velocity was set equal to the local gas injection velocity.

Influence of Grid Refinement

A grid influence is apparent between the different meshes, more specifically in the diverging part of the nozzle where a classical particle-free zone is observed. In the combustion chamber, the differences are quite small and remain acceptable. Nevertheless, the coarse mesh was rejected and the simulations were performed with the intermediate one. The differences observed with the fine one are negligible and they do not justify the increase in CPU time.

Influence of the Particle Injection Velocity

At this point, the injection velocity of the particles from the propellant surface is equal to the gas-phase one. This quantity is very important because it will determine the number density of particles entering the flow. Indeed the specific dispersed mass flow rate is given by the relation

$$\dot{M}_p = n4/3\pi R_p^3 U_{p,\text{inj}} \rho^*_{\text{Al}}$$

Because of the parabolic nature of the system of equations of the dispersed phase, the value of each quantity must be imposed at the propellant surface. The particle radius R_p is fixed easily, requiring a choice between the number density and the velocity. The velocity appears to be a more natural parameter to impose. It is not an easy task to specify a value but it is reasonable to assume that the velocity is in the range of the propellant burning rate, $\approx 10^{-2}$ m/s and the gas velocity. In Ref. 12, the specified velocity is imposed to be 1% of the gas velocity. The values chosen in this study are, 1, 10, 25, 35, 50, 65, 75, and 100%, and the particle diameter is 30 μm.

For inert particles, it was shown that the injection velocity does not influence the flowfield.[4] The most affected quantity is the combustion thickness δ. As the injection velocity increases, the thickness of the combustion zone increases. Because of a higher initial impulse, the combustion of a particle occurs along a longer path than with a low injection velocity (see Table 3). This phenomenon leads to a modification of the gas temperature distribution in the combustion chamber, as shown in Fig. 5, and thus a changing of the average gas temperature in the combustion chamber. In Fig. 6, the average

Table 3 Influence of dispersed-phase injection velocity

u_p/u_g, %	τ_c, ms	δ
1	2.84	0.60
10	2.83	0.59
25	2.84	0.61
35	2.83	0.65
50	2.80	0.65
65	2.80	0.68
75	2.79	0.72
100	2.73	0.73

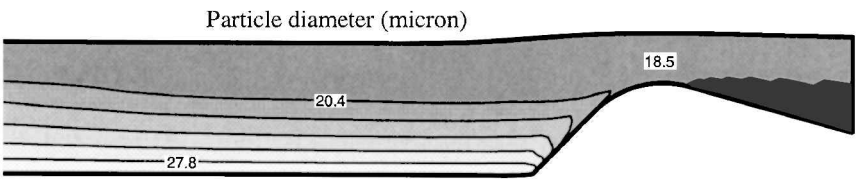

Fig. 4 Distribution of particle, diameter contours at steady state, using Hermsen's model (injected particles' diameter = 30 θ m, average diameter at exit nozzle = 19.3 θ m).

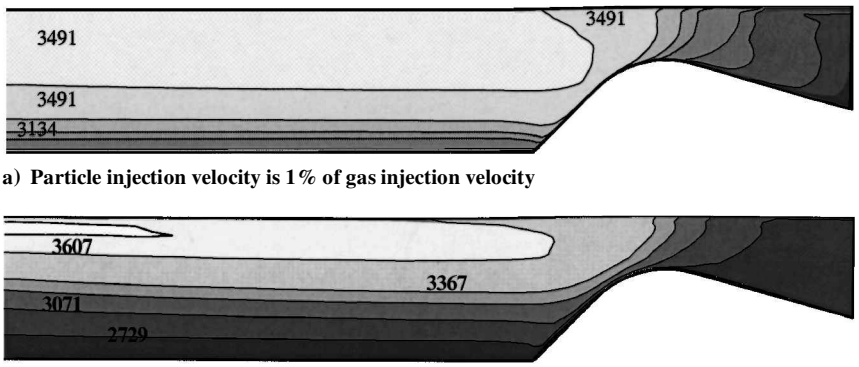

a) Particle injection velocity is 1% of gas injection velocity

b) Particle injection velocity is 100% of gas injection velocity

Fig. 5 Distribution of gas temperature at steady state (30-θ m particles).

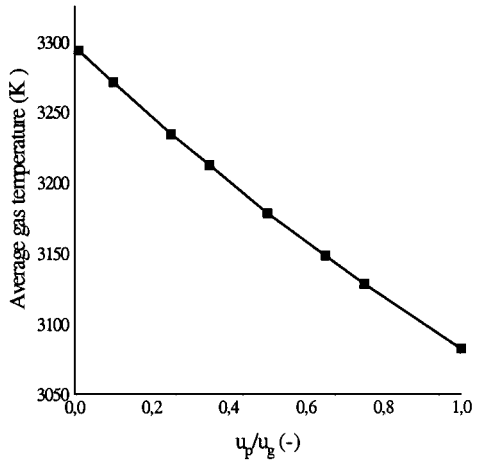

Fig. 6 Average gas temperature at steady state in the combustion chamber vs injection velocity ratio (30-θ m particles).

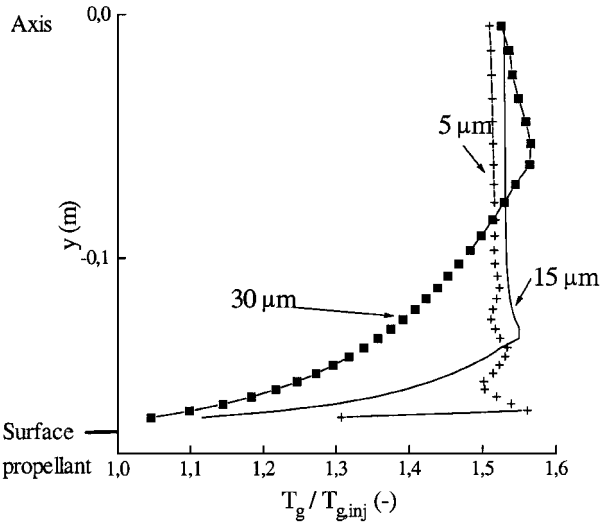

Fig. 7 Dimensionless gas temperature ($T_g/T_{g,\text{inj}}$) profiles at steady state (cross section at the midpoint of the propellant surface; injected particle diameter = 5, 15, and 30 θ m).

gas temperature is plotted relative to the ratio of injection velocities, and a linear variation is observed. Even though this influence is not negligible, it not as important as suggested by Fig. 6. Indeed, for an injection velocity multiplied by 100 (1–100%), the final average temperature is only multiplied by 0.93.

There is no significant influence on the pressure, but these values are not reported.

From Table 3, note that there is also no influence on the combustion time. The observed differences are not significant and may be due to a particle trajectory calculation that is not sufficiently accurate.

It is clear that the particle injection velocity, which is quite difficult to determine, has a nonnegligible influence. Even though the most important parameters (pressure, combustion time, and average temperature) are not really modified, the combustion thickness depends on this ratio. Also, δ is an important parameter because, to perform correct acoustic analysis, the temperature must be constant to determine a reference speed of sound. That only occurs above the combustion zone.

Influence of Particle Diameter

The influence of the initial particle diameter also was studied. In this case, the gas temperature field obviously will be modified. The burning rate implies that the smallest particles burn close to the propellant surface whereas the largest burn for a longer time, causing a broadening of the combustion. Four diameters were chosen: 5, 15, 30, and 40 μm. The injection velocity was set equal to 25% of the gas velocity. In Table 4, the combustion time and the average gas temperature are reported, except for the 40-μm size particles, which burn out near the exit cross section.

In Fig. 7, the dimensionless gas temperature $T/T_{g,\text{inj}}$ is plotted for each diameter studied. This graph is related to an abscissa at the midpoint of the combustion chamber and for the steady state. As expected, small particles (5 μm) burn near the surface of the propellant. Actually, 5-μm particles burn as soon as they enter the motor: an increase of temperature is observed until the equilibrium temperature is reached. An oscillation is observed but it may be due to a numerical behavior rather than a physical one. The source term due to the heat released is very high and may lead to some numerical oscillations; additional numerical experiments could clarify this point.

Note also that the different profiles give quite similar results, considering the temperature reached after combustion. The difference observed between the steady-state values is less than 3% ($\approx$100 K): The mass of aluminum injected is the same and thus also is the chemical heat released in the gas. The difference may be due to the convective heat transfer between the gas and inert alumina particles. For 40-μm particles, the analysis is quite different because the combustion is complete only in the diverging part of the nozzle.

The time evolution of the 30-μm-diam particles was analyzed. At steady state, the trajectory of pseudoparticles injected from half of the propellant surface was computed and the diameter was plotted relative to time (along a particle path). Analytical D^n laws also were computed using $D^n = D_0^n - kt$, and it was assumed that when $t = \tau_c$, the diameter was the residual size of the alumina particle D_{res} (this value was determined from the numerical results). Then k obeys the relation

$$k = \frac{D_{\text{res}}^n - D_0^n}{\tau_c}$$

Table 4 Influence of particle initial diameter

$D_{p,\text{inj}}$, μm	τ_c, ms	$\bar{T}$, K
5	0.1	3503
15	0.82	3433
30	2.841	3234
40	*	*

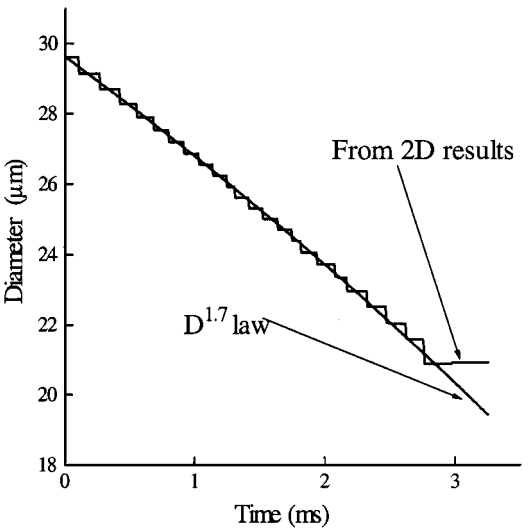

Fig. 8 Evolution of the diameter vs combustion times of a particle injected from the half of the propellant surface (two-dimensional results and analytical $D^{1.7}$ law vs time).

By calculating the global error between the analytical law and the two-dimensional results, $n = 1.7$ appears to be the best value, although, according to Brooks and Beckstead,[11] a D^2 law seems to hold. The combustion time is too short to magnify the differences between the curves. In Fig. 8, the time evolution of the diameter along a particle trajectory is compared to the $D^{1.7}$ fit.

When the combustion is over, the size of the particle remains constant in the two-dimensional computation whereas, when the results are fitted with a D^n law, the size varies.

Influence of Oxidation Efficiency Parameter *E*

The chemical mechanism of the aluminum combustion, Eq. (2), only involves O_2 as oxidizer species although it appears in low proportions in the combustion products. Therefore, O_2 may come from dissociated species, such as CO_2, or from H_2O, and so, an efficiency parameter is defined to take into account the effective presence of oxygen (see Governing Equations). An exhaustive study was not performed; only the influence of the parameter E was assessed. Two values, based on E_{CO_2} and E_{H_2O} from Table 1, are used. With the corresponding mass fraction, it leads to the following numerical values: $E_{\text{Beckstead}} = 0.389$, $E_{\text{Marion}} = 0.493$ (Table 1). For the lower value, the calculations diverged and no results were obtained, and so, an arbitrary value of 0.75 also was tested. Then, some comparisons with previous results with $E = 1$ also could be made.

Some 30-μm particles were injected in the flow. As the efficiency diminished, the combustion time increased, not a surprising result. Therefore, for low value of E, the combustion process is not completed at the exit cross section. The only result that was analyzed was for $E = 0.75$ (see Table 5).

The combustion τ_c increases but not in the same ratio as the efficiency E. Whereas E is multiplied by 0.75, τ_c is multiplied by 1.16. Two remarks can be made about the results, which are not intuitive. When the efficiency is reduced, the average gas temperature is increases slightly and the residual size of the alumina at the nozzle exit (D_{exit}) decreases. The physical interpretation is not clear because the influence of E is very nonlinear. However this parameter may help in tuning the model to fit some experimental data.

Table 5 Influence of combustion efficiency

$E(-)$	τ_c, ms	$\bar{T}$, K	D_{exit}, μm
1	2.841	3234	21.1
0.75	3.3	3253	20.5

Concluding Remarks

Although this parametric study is not exhaustive, several trends are evident. The injection velocity of the particles has a limited influence on the average quantities of the gas as well as the particle combustion time. However, the distribute combustion zone (its thickness) is very dependent on this parameter. Thus, this particular velocity should be measured carefully. The initial diameter of the particles entering the flow also has a part in the distribute combustion, but, here again, the mean average gas quantities are little affected by the variation of this parameter: The total mass of aluminum entering the flow, and thus the potential chemical energy, is the same whatever the value of the diameter or the injection velocity. The combustion efficiency results are less general than the two previous ones because they are linked to one specific model, the Law model.

Conclusions

Modeling two-phase reactive flows, including the combustion of aluminum particles in an SRM environment, requires an efficient numerical algorithm.

An analysis of two existing combustion models is presented. It is clear that both models, Hermsen and Law, do not take into account some of the real phenomena occurring. Nevertheless, incorporating such models in numerical algorithms for two-phase unsteady compressible flows leads to solutions that are generally correct when compared with chemical equilibrium calculations.

A reduced model for the gas-phase composition is used because it is not realistic to compute the transport of each gaseous species, in addition to the burning particles. This is based on the analysis of the chemical equilibrium composition of propellant with and without aluminum.

An Eulerian approach for the dispersed phase is used. This approach seems more appropriate for computations of unsteady flows. Although a Lagrangian method can provide similar results, these require much memory and CPU capacity to compute unsteady large-scale SRM environments motor. Basically, Eulerian approach is preferred here because such methods offer a more efficient way to carry out numerous parametric studies, which are still needed.

The model works well enough to help in the understanding of parameters that are not well known. The basic description of the combustion is preserved, including the consumption of oxidizer and the gain of products as well as the global mass conservation. According to the numerical results, the gas temperature distribution is very different from a one-phase flow calculation; i.e., the highest temperature is not reached at the propellant surface but at a non-negligible distance from it because of the time required to burn aluminum particles entering the flow. It also is pointed out that the distribute combustion (vs surface combustion) is dependent on two-phase parameters such as the initial particle velocity and the particle diameter. These quantities generally are not well measured, but they are required as known input in order to perform more complex numerical experiments.

Acknowledgments

This work received financial support from the CNES/DLA on the internal flows in the SRM (ASSM Project). Helpful discussions with J. Dupays of ONERA and all others researchers involved in ASSM project as well as with my colleagues at IUSTI are acknowledged. Acknowledgment also goes to H. Krier, University of Illinois, who spent time to correct the English.

References

[1] Sabnis, J., de Jong, F., and Gibeling, H., "A Two-Phase Restricted Equilibrium Model for Combustion of Metalized Solid Propellants," AIAA Paper 92-3509, July 1992.

[2]Liaw, P., and Chen, Y. S., "Particulate Multi-Phase Flowfield Calculation with Combustion, Break-Up Models for Solid Rocket Motor," AIAA Paper 94-2780, June 1994.

[3]Hermsen, R. W., "Aluminum Combustion Efficiency in Solid Rocket Motors," AIAA Paper 81-0038, July 1981.

[4]Vuillot, F., Basset, T., Dupays, J., Daniel, E., and Lupoglazoff, N., "2D Navier–Stokes Stability Computation for Solid Rocket Motors: Rotational, Combustion and Two-Phase Flow Effects," AIAA Paper 97-3326, July 1997.

[5]Law, C. K., "A Simplified Theoretical Model for the Vapor-Phase Combustion of Metal Particles," *Combustion Science and Technology*, Vol. 7, No. 3, 1973, pp. 197–212.

[6]Basset, T., Daniel, E., and Loraud, J.-C., "Etudes Théoriques et Numériques sur la Combustion de Particules d'Aluminium," *Canadian Journal of Chemical Engineering*, Vol. 75, 1997, pp. 938–948.

[7]Glassman, I., "Combustion of Metals, Physical Consideration," *Progress in Astronautics and Rocketry*, Vol. 1, 1960, pp. 253–257.

[8]Kuehl, D. K., "Ignition and Combustion of Aluminum and Beryllium," *AIAA Journal*, Vol. 3, No. 12, 1965, pp. 253–257.

[9]Dreizin, E. L., "Experimental Study of Stages in Aluminum Particle Combustion in Air," *Combustion and Flame*, Vol. 105, 1996, pp. 541–556.

[10]Marion, M., "Etude de la Combustion des Particules d'Aluminium sous Pression," Ph.D Thesis, Université d'Orléans, Univ. d'Orléans, France, Dec. 1996.

[11]Brooks, K. P., and Beckstead, M. W., "Dynamics of Aluminum Combustion," *Journal of Propulsion and Power*, Vol. 11, No. 4, 1995, pp. 769–780.

[12]Davis, A., "Solid Propellants: The Combustion of Particles of Metal Ingredients," *Combustion and Flame*, Vol. 7, No. 12, 1963, pp. 359–367.

[13]Widener, J. F., and Beckstead, M. W., "Aluminum Combustion Modeling in Solid Propellant Combustion Products," AIAA Paper 98-3824, July 1998.

[14]Liang, Y., and Beckstead, M. W., "Numerical Simulation of Unsteady, Single Aluminum Particle Combustion in Air," AIAA Paper 98-3825, July 1998.

[15]Ishii, R., Umeda, Y., and Yuhi, M., "Numerical Analysis of Gas-Particle Two-Phase Flows," *Journal of Fluid Mechanics*, Vol. 203, 1989, pp. 475–515.

[16]Daniel, E., Saurel, R., Larini, M., and Loraud, J.-C., "A Multiphase Formulation for Two-Phase Flows," *International Journal of Heat and Fluid Flow*, Vol. 4, No. 3, 1994, pp. 269–280.

[17]Daniel, E., Basset, T., and Loraud, J. C., "Combustion de Particules d'Aluminium," Commande ONERA/IUSTI 724.918/DA.B11DC, Palaiseau, France, 1997.

[18]Price, E. W., "Combustion of Metalized Propellants," *Fundamentals of Solid Propellants Combustion*, edited by K. K. Kuo and M. Summerfield, Vol. 90, Progress in Astronautics and Aeronautics, AIAA, New York, 1984, pp. 479–513.

[19]Glassman, I., "Combustion of Metals Revisited Thermodynamically," *Proceeding of the Eastern States Section of the Combustion Institute*, Princeton, NJ, 1993, pp. 17–26.

[20]Faeth, G. M., "Current Status of Droplet and Liquid Combustion," *Proc. Energy Combustion Science*, Pennsylvania State Inst., University Park, Vol. 3, 1977, pp. 191–224.

[21]Clift, R., Grace, J. R., and Weber M. E., *Bubbles, Drops and Particles*, Academic, New York, 1978.

[22]Chang, I. S., "One and Two-Phase Nozzle Flows," *AIAA Journal*, Vol. 18, No. 12, 1980, pp. 1455–1461.

[23]Dash, S. M., and Thorpe, R. D., "Shock Capturing Model for One- and Two-Phase Supersonic Exhaust Flow," *AIAA Journal*, Vol. 19, No. 7, 1981, pp. 842–851.

[24]Dupays, J., Prevost, M., Tarrin, P., and Vuillot, F., "Effects of Particulate Phase on Vortex Shedding Driven Oscillations in Solid Rocket Motors," AIAA Paper 96-3248, July 1996.

[25]Toro, E. F., *Riemann Solvers and Numerical Methods for Fluid Dynamics*, Springer–Verlag, Heidelberg, 1997.

[26]Saurel, R., Daniel, E., and Loraud, J.-C., "Two Phase Flows: Second Order Schemes and Boundary Conditions," *AIAA Journal*, Vol. 32, No. 6, 1994, pp. 1214–1221.

[27]Lupoglazoff, N., and Vuillot, F., "Numerical Simulation of Nonsteady Two-Dimensional Flows in Solid Propellant Propulsion System," *Recherche Aerospatiale*, No. 2, 1992, pp. 21–41.